Fluoride removal from water using a magnesia-pullulan composite in a continuous fixed-bed column

Yuanyao Ye[a,b], Jing Yang[c], Wei Jiang[a*], Jianxiong Kang[a*], Ying Hu[d], Huu Hao Ngo[b], Wenshan Guo[b], Yiwen Liu[b]

[a]*School of Environmental Science and Engineering, Huazhong University of Science and Technology, No. 1037 Luoyu Road, Wuhan 430074, PR China*

[b]*Centre for Technology in Water and Wastewater, School of Civil and Environmental Engineering, University of Technology Sydney, Sydney, NSW 2007, Australia*

[c]*The IT Electronics Eleventh Design & Research Institute Scientific and Technological Engineering Corporation Limited*

[d]*Yangtze Memory Technologies Co., Ltd*

**Corresponding author. Tel: +86 02787792512. Fax: +86 02787792172*

E-mail address: jiangwei0707@hust.edu.cn & jxkang@hust.edu.cn

Abstract

A magnesia-pullulan composite (MgOP) was previously shown to effectively remove fluoride from water. In the present study, a continuous fixed-bed column was used to examine the application of the composite at an industrial scale. The influencing parameters included bed mass (4.0, 6.0 and 8.0 g), influent flow rate (8, 16 and 32 mL/min), inlet fluoride concentration (5, 10 and 20 mg/L), reaction temperature (20, 30 and 40 °C), influent pH (4, 7 and 10) and other existing anions (HCO_3^-, SO_4^{2-}, Cl^- and NO_3^-), through which the breakthrough curves could be depicted for the experimental data analysis. The results indicated that MgOP is promising for fluoride removal with a defluoridation capacity of 16.6 mg/g at the bed mass of 6.0 g, influent flow rate of 16 mL/min and inlet fluoride concentration of 10 mg/L. The dynamics of the fluoride adsorption process were modeled using the Thomas and Yan models, in which the Yan model presented better predictions for the breakthrough curves than the Thomas model. Moreover, the concentration of magnesium in the effluent was monitored to determine Mg stability in the MgOP composite. Results indicated the effluent concentration of Mg^{2+} ions could be kept at a safe level. Calcination of fluoride-loaded MgOP effectively regenerated the material.

Keywords: MgOP; defluoridation; breakthrough curve; fixed-bed column; desorption and regeneration.

1. Introduction

Fluoride is an essential micronutrient because a trace intake of fluoride (0.4–0.6 mg/L) is helpful for normal mineralization of bones and formation of dental enamel. However, excessive concentrations of fluoride in drinking water may result in a progressive crippling disease known as fluorosis. The optimum fluoride level in drinking water set by the World Health Organization (WHO) is < 1.5 mg/L (WHO, 2011). Fluoride in the aquatic environment is derived mainly from natural weathering of fluorine-containing minerals such as fluorapatite and fluorite, industrial activities such as the production of glass and semiconductors, and mineral processing (Wang et al., 2017). More than 200 million people globally are exposed to drinking water containing > 1.5 mg fluoride/L (Chai et al., 2013). Fluoride contamination has serious effects on the geo-environment in many countries, and especially in developing countries (Mohan et al., 2017).

Various technologies for defluoridation based on the principle of adsorption, precipitation-coagulation and the membrane separation process have been developed or are at the development stage. Primarily lime and aluminum salts are utilized to remove fluoride from water in the precipitation-coagulation process; the resulting fluoride-based precipitates achieve satisfactory fluoride removal. However, the method may also produce an excessive quantity of surplus sludge and thus increase the overall operation costs. Moreover, the use of aluminum salts may release some aluminum ions to the water in the defluoridation process. Consequently, human health can be detrimentally affected because the excessive aluminum concentrations (> 0.2 mg/L) may cause diseases such as dementia (Shrivastava and Vani, 2009).

Membrane separation processes can effectively concentrate the negatively charged and highly hydrated fluoride ions within the reactor (Chakrabortty et al., 2013; Shen and Schäfer, 2014). Membrane separation can reduce costs and offer a viable treatment option in locations

where resources or access to technology are limited (Jadhav et al., 2015). A major challenge is fluoride removal from the reactor after treatment and further research is needed to solve this problem.

Thus, adsorption is probably the most promising method for fluoride removal in drinking water treatment because of its simple design and operation, high efficiency and low costs compared with other methods (Kameda et al., 2015; Ye et al., 2016). More importantly, adsorption is more likely to be utilized for fluoride removal in less developed countries, where advanced wastewater treatment is unavailable.

Effective low-cost materials, including activated alumina and carbon, rare earths and magnesia (MgO), have been examined for defluoridation (Jadhav et al., 2015; Kameda et al., 2017; Loganathan et al., 2013). MgO is one of the most widely used materials and, unlike alumina, does not introduce potentially harmful substances to the water during treatment. However, MgO has disadvantages that may inhibit its commercial application for defluoridation (Thergaonkar and Nawalakhe, 1971) including: (i) pressure drop in the column due to its use in powder form; (ii) long time required to achieve equilibrium; and (iii) high pH of the treated water. Many researchers have developed MgO-based adsorbents for fluoride removal by adding other materials. For example, Xu et al. (2011) prepared MgO-loaded fly ash cenospheres that achieved maximum defluoridation capacity of approximately 6.0 mg/g at the initial fluoride concentration of 100 mg/L, but fluoride adsorption was inhibited by increasing pH. Granular matrix-supported nano-MgO was developed that could achieve effective fluoride removal from water; however, the fluoride adsorption on the adsorbent required more than 350 min to reach equilibrium when the initial fluoride concentration was 2.5 to 30 mg/L (Oladoja et al., 2015). Sundaram et al. (2009) revealed that the combination of chitosan and MgO resulted in a bio-composite adsorbent that was shown to have high adsorption capacity for fluoride ions and short equilibrium time due to a large number of

hydroxyl groups in the chitosan.

In the previous study, pullulan (a biodegradable extracellular water-soluble microbial polysaccharide) was found to have highly biocompatible and non-toxic properties; thus, the material potentially could be employed as an adsorbent (Kang et al., 2011). More hydroxyl groups were found in the pullulan saccharide unit than in the chitosan saccharide unit, for which the number of potential sites for adsorption could be increased. In the previous study (Kang et al., 2011), pullulan was spread on MgO to synthesize a magnesia-pullulan composite (MgOP) and fluoride adsorption on the MgOP was explored in a batch system. Compared to other similar adsorbents, the accessibility of the adsorbate-binding sites was increased and the defluoridation capacity of MgOP was hence enhanced to 7.17 mg/g at the initial fluoride concentration of 15 mg/L and an adsorbent concentration of 2 g/L. Moreover, the fluoride adsorption on MgOP reached equilibrium within 60 min at a wide range of initial fluoride concentrations. Furthermore, effective fluoride removal was achieved over a wide pH range (2–12).

A continuous flow system is required for fluoride removal at a treatment plant scale. A fixed-bed column filter is considered optimum for removing excess fluoride from water and has the advantages of operational simplicity, cost effectiveness, and regeneration capability (García-Sánchez et al., 2017; Roy et al., 2017).

The aim of this study was to evaluate MgOP performance with respect to fluoride removal in a continuous fixed-bed column and provide guidance for design and operation of the reactor. MgOP performance was evaluated under various operating parameters, including bed mass, volumetric flow rate, influent fluoride concentrations, reaction temperature, inlet pH and the presence of coexisting anions. Models developed by Thomas (1944) and Yan et al. (2001) were used to describe the breakthrough curves. Magnesium concentrations were determined to ensure high-quality treated water. MgOP regeneration was explored for process

sustainability and economic feasibility

2. Materials and methods

2.1 MgOP preparation

The MgOP was prepared according to the sol-gel method used in our previous study (Kang et al., 2011). This entailed adding 8.0 g of MgO (Sinopharm Chemical Reagent Co., Ltd, Shanghai, China) and 12.0 g of pullulan (Shandong Freda Biotechnology Co., Ltd, Linxi, China) to deionized water in a 1000-mL polypropylene beaker (weight ratio MgO: pullulan = 2:3). After 24 h of stirring at room temperature, the aqueous mixture was dried at 105 °C in an oven for 12 h and then calcined at 450 °C in a muffle furnace for 2 h to obtain the composite MgOP. The MgOP was pulverized, sieved and stored in a sealed bag for later use.

2.2 Analytical methods

Sodium fluoride (NaF) was used to prepare a standard fluoride solution (1000 mg/L), which could be diluted to obtain the desired concentrations of working fluoride solutions. The fluoride concentrations were tested through the ion selective electrode method using an ion meter and electrodes (Shanghai branch pXS-215, Tianda Instrument Shanghai Co., Ltd., Shanghai, China). Furthermore, NaOH and HCl solutions (0.1 mol/L) were used to adjust the pH values of fluoride solutions, and a pH meter (pHS-3C, Shanghai REX Instrument Factory Co., Ltd., Shanghai, China) was utilized for monitoring pH changes. An atomic absorption spectrophotometer was utilized to measure the effluent magnesium concentrations (ZEEnit700P, Analytik Jena AG, Jena, Germany).

2.3 Fixed-bed column study

The performance of MgOP for fluoride removal from water was evaluated using duplicate laboratory-scale continuous fixed-bed columns. Each fixed-bed adsorption filter column consisted of an organic glass (i.e., poly(methyl methacrylate)) cylinder having an internal diameter and height of 4 and 20 cm, respectively. Prior to adding the MgOP

adsorbent, glass wool (~10 cm) was fixed in place at the bottom of cylinder and then compacted using a glass rod. The glass wool served as packing to a) facilitate an even distribution of flow across the column cross-section; b) prevent loss of adsorbent; and c) ensure a closely packed arrangement of MgOP.

MgOP was first washed using deionized water to remove the powder from the MgOP surface and avoid subsequent blocking of the bed and glass filter. An appropriate mass (4.0, 6.0 or 8.0 g) of washed MgOP (particle size distribution ranging from 420 to 840 μm) was then added to the column and packed by fully immersing the material in deionized water. Using this procedure, MgOP was compacted by natural gravity settlement, forming a uniform bed and ensuring a complete expulsion of air bubbles.

The fluoride solution was pumped downward through the MgOP bed. The influent volumetric flow rate varied by experiment but was held constant throughout a given experiment using a variable flow peristaltic pump (BT 100-1F, Baoding Longer Precision Pump Co., Ltd., Baoding, China). Steady flow through the column was assured by periodically recording the time taken to collect 100 mL of treated solution. Effluent samples were collected at different time intervals, filtered through a 0.45-μm membrane filter (Tianjin Jinteng Experimental Equipment Co. Ltd., Tianjin, China), and then analyzed for residual fluoride concentrations and pH to determine the breakthrough curves.

The experimental temperature was kept constant by maintaining the columns in a water bath. Breakthrough curves were determined for experimental variables that included bed mass (i.e. adsorbent mass) (4.0, 6.0 and 8.0 g), volumetric flow rate (8.0, 16.0 and 32.0 mL/min), influent fluoride concentration (5, 10 and 20 mg/L), reaction temperature (20, 30 and 40 °C), inlet pH (4, 7 and 10) and various concentrations (0, 250 and 500 mg/L) of other coexisting anions (Cl^-, SO_4^{2-}, NO_3^-, and HCO_3^- ions).

2.4 Data analysis

The breakthrough curves were used to assess the performance of the MgOP bed in removing fluoride. The breakthrough curves were expressed as the ratio between influent adsorbate concentration (C_0) and effluent adsorbate concentration (C_t) as a function of the volume of treated water. The dynamic column capacity was calculated using Eqs. (1) and (2):

$$q_e = \frac{Q}{1000m}\int_{t=0}^{t=t_{total}}(C_0 - C_t)dt \quad (1)$$

$$q_b = \frac{Q}{1000m}\int_{t=0}^{t=t_b}(C_0 - C_t)dt \quad (2)$$

where q_e and q_b (mg/g) are the dynamic column capacity at exhaustion point and the breakthrough point, respectively; t_{total} (h) and t_b (h) are the exhaustion time and breakthrough time, respectively, and defined as the time taken to reach $C_t/C_0 = 0.8$ and $C_t/C_0 = 0.1$, respectively; Q (mL/min) is the volumetric flow rate in the continuous fixed-bed column; and m (g) is the dry weight of MgOP in the column.

Each dynamic adsorption experiment was conducted in duplicate using parallel columns. The data variance derived from each of the duplicate column experiments was determined to be negligible. Experimental data derived from the breakthrough curves were used to optimize the operation and design parameters of the column. Furthermore, mathematical models were employed to describe the experimental data and predict the column performance. The Thomas and Yan models were used to describe the breakthrough curves.

2.5 Desorption and regeneration of MgOP

To increase the economic feasibility of MgOP for commercial application, desorption and regeneration experiments of MgOP were explored in a batch mode. According to previous research (Kang et al., 2011), fluoride-adsorbed MgOP was obtained when the initial fluoride concentration was 10 mg/L and the contact time was 60 min at 2.0 g/L MgOP, which was used in the desorption study. In the current desorption study, 100 mL of various solvents (i.e. deionized water, HCl, NaCl, $C_6H_8O_7$, $Na_3C_6H_5O_7$, NaOH, and Na_2CO_3 solutions) were

187 added to polyethylene tubes containing 0.2 g of dry, fluoride-loaded MgOP. The mixture was
188 continuously stirred at 150 rpm for 24 h at room temperature and then filtered through a 0.45-
189 μm membrane (Tianjin Jinteng Experimental Equipment Co. Ltd., China). The fluoride
190 concentrations of the resulting filtrate were tested. The concentration of desorbing agents
191 expected for deionized water was 0.1 M and the pH of desorbing agents was controlled to be
192 above 3 to avoid the possible dissolution of MgOP. The desorption efficiency (DE) was
193 calculated using Eq. (3):

194 $$DE = \frac{A_d}{A_0} \times 100\% \quad (3)$$

195 where A_d (mg/g) and A_0 (mg/g) are the adsorption capacity of the desorbed and original
196 adsorbent, respectively.

197 After desorbing fluoride from the fluoride-loaded MgOP using the solvents mentioned
198 above, the resulting MgOP was washed three times with deionized water and dried at 105 °C
199 for 12 h. The desorbed, washed MgOP (0.2 g) was added to polyethylene tubes containing
200 100 mL of solution containing 10 mg fluoride/L. The mixture was shaken at 150 rpm for 24 h
201 at room temperature and filtered, after which the concentration of fluoride in the mixture was
202 measured. The regeneration efficiency (RE) was calculated using Eq. (4):

203 $$RE = \frac{A_r}{A_0} \times 100\% \quad (4)$$

204 where A_r (mg/g) and A_0 (mg/g) are the adsorption capacity of the regenerated material and
205 original adsorbent, respectively.

206 Fluoride-loaded MgOP was also regenerated by calcination for 60 min at 500 °C in the
207 absence of air. The resulting solid (0.2 g) was added to polyethylene tubes with 100 mL of
208 solution containing 10 mg·fluoride/L. The mixture was shaken at 150 rpm for 24 h at room
209 temperature, after which the suspension was filtered and fluoride content measured. In the
210 regeneration study, only RE could be determined. The properties of MgOP and fluoride-
211 adsorbed MgOP before and after calcination were characterized with X-ray diffraction

(XRD), Fourier Transform Infrared (FTIR) spectroscopy and Scanning Electron Microscopy (SEM). Cu Kα radiation was employed to study the XRD patterns (Empyrean, PAN analytical B.V., Almelo, Holland) and the IR spectrum was obtained using an FTIR spectrophotometer (VERTEX 70, Bruker Corporation, Karlsruhe, Germany). A Quanta 200 (FEI Company, Hillsboro, America) instrument was used to obtain SEM images.

3. Results and discussion

3.1 Breakthrough analysis

Bed mass, volumetric flow rate and inlet adsorbate concentration are crucial for efficient column design and operation, and these factors affect the breakthrough, or discharge, of fluoride. The shape of breakthrough curves also can be affected by environmental factors including reaction temperature, pH and the presence of other anions.

Our previous work (Kang et al., 2011) showed that fluoride adsorption on MgOP follows the Langmuir isotherm and pseudo second-order kinetics. Since the Thomas model (Thomas, 1944) assumes Langmuir kinetics of adsorption-desorption with no axial dispersion, and the rate driving force obeys second-order reversible reaction kinetics (Reynolds, 1977), the model was used to analyze the experimental data. The model is expressed as Eq. (5):

$$\frac{C_t}{C_0} = \frac{1}{1+\exp[\frac{k_T}{Q}(q_T m - C_0 V)]} \quad (5)$$

where C_t (mg/L) is the effluent concentration of adsorbate; C_0 (mg/L) is influent concentration of adsorbate; Q (mL/h) is volumetric flow rate; m (g) is dry adsorbent mass; k_T (mL/h/mg) is the kinetic rate constant of the Thomas model; q_T (mg/g) is maximum adsorption capacity calculated by the Thomas model; and V (L) is the volume of treated water.

The Thomas model has a limitation in that it predicts a fixed effluent concentration when time t is zero. An empirical model proposed by Yan et al. (2001) overcomes this

limitation, so the Yan model also was utilized for analyzing the experimental data. The model of Yan et al. (2001) is expressed as Eq. (6):

$$\frac{C_t}{C_0} = 1 - \frac{1}{1+(\frac{Q}{k_Y q_Y m}V)^{(k_Y c_0/Q)}} \quad (6)$$

where k_Y (mL/h/mg) is the kinetic rate constant of the Yan model; q_Y (mg/g) is maximum adsorption capacity estimated by the Yan model and other parameters are as defined for the Thomas (1944) model.

Values for parameters in the two models were determined by analysing the fluoride breakthrough curves and are given in Table 1.

Table 1

Thomas (1944) and Yan et al. (2001) model constants for fluoride adsorption on MgOP.

Conditions	Yan model				Thomas model				t_b (h)	q_b (mg/g)	q_e (mg/g)
	k_Y (mL/h/mg)	q_Y (mg/g)	t_{bY} (h)	R^2	k_T (mL/h/mg)	q_T (mg/g)	t_{bT} (h)	R^2			
bed mass (g)											
4	170.4	5.14	1.1	0.991	46.4	10.43	-	0.908	1.4	3.23	13.1
6	174.1	6.96	2.3	0.967	24.2	14.17	-	0.849	3.6	5.65	16.6
8	220.0	6.45	4.5	0.985	20.0	15.98	2.3	0.918	6.1	7.13	17.0
volumetric flow rate (mL/min)											
8	83.2	7.91	2.3	0.987	10.2	16.31	-	0.899	6.6	5.16	17.4
16	174.2	6.97	2.3	0.966	24.2	14.16	-	0.849	3.6	5.65	16.6
32	344.3	4.77	1.5	0.995	66.8	9.79	-	0.921	1.0	3.05	12.4
inlet initial fluoride concentration (mg/L)											
5	305.0	6.07	2.9	0.980	25.9	11.29	-	0.851	6.0	4.49	14.0
10	174.2	6.97	2.3	0.966	24.2	14.16	-	0.849	3.6	5.65	16.6
20	85.5	5.44	0.8	0.980	31.3	10.91	-	0.880	0.9	2.81	14.4
reaction temperature (°C)											
20	181.2	6.53	2.3	0.981	26.1	13.69	0.1	0.884	3.3	5.10	16.0
30	174.2	6.97	2.3	0.966	24.2	14.16	-	0.849	3.6	5.65	16.6
40	167.0	8.34	2.5	0.975	19.9	16.47	-	0.861	3.7	5.69	18.0
pH											
4	210.9	6.56	3.2	0.975	26.6	15.57	1.4	0.893	4.4	6.85	17.9
7	171.5	6.10	1.9	0.976	27.7	12.25	-	0.869	2.9	4.63	15.2
10	221.9	5.85	3.1	0.974	30.7	14.41	1.8	0.900	4.4	6.86	17.0
coexisting anions											
0	174.2	6.97	2.3	0.966	24.2	14.16	-	0.849	3.6	5.65	16.6
Cl^- (250 mg/L)	183.6	7.92	2.9	0.973	21.3	16.87	0.2	0.869	4.2	6.35	18.8
Cl^- (500 mg/L)	199.4	6.88	3.0	0.982	25.0	15.62	0.9	0.900	4.1	6.26	18.6
SO_4^{2-} (250 mg/L)	160.0	12.00	3.2	0.982	15.7	22.31	-	0.879	4.6	7.10	22.1
SO_4^{2-} (500 mg/L)	166.7	10.38	3.0	0.978	17.2	20.23	-	0.869	4.3	6.95	20.8
NO_3^- (250 mg/L)	204.1	5.84	2.6	0.986	29.7	13.51	1.0	0.914	3.6	5.57	16.0
NO_3^- (500 mg/L)	192.9	6.60	2.7	0.986	25.9	14.57	0.6	0.905	3.6	5.62	16.9
HCO_3^- (250 mg/L)	292.5	2.03	1.8	0.998	74.7	6.65	1.2	0.989	1.9	3.06	7.1
HCO_3^- (500 mg/L)	398.8	0.83	1.2	0.998	189.7	3.56	1.0	0.993	1.2	1.83	3.7

3.1.1 Bed mass

The effects of bed mass (i.e., adsorbent mass) (4.0, 6.0, and 8.0 g) on breakthrough curves were explored at a fixed influent flow velocity of 16 mL/min and influent fluoride concentration of 10 mg/L. The shapes of breakthrough curves resulting from use of the different bed masses were quite similar (Fig. 1). The volume of treated water at breakthrough

point increased from 1.3 to 5.9 L as the bed mass increased from 4.0 to 8.0 g. The possible reason for this is that in flow through a fixed bed, diffusion mass transfer is predominant compared to the axial dispersion phenomenon at greater bed mass (Abdolali et al., 2017). Thus, at the higher bed mass, the fluoride ions had sufficient time to diffuse into the entire mass of MgOP, which indicated the residence time of fluoride ions in the column increased. Moreover, the defluoridation capacity of MgOP at exhaustion time also increased from 13.1 to 17.0 mg/g as the bed mass varied from 4.0 to 8.0 g. A greater bed mass increases adsorbent area but also increases bed resistance, which may detrimentally influence fluoride adsorption. Hence, 6.0 g of bed mass was utilized in the subsequent experiments.

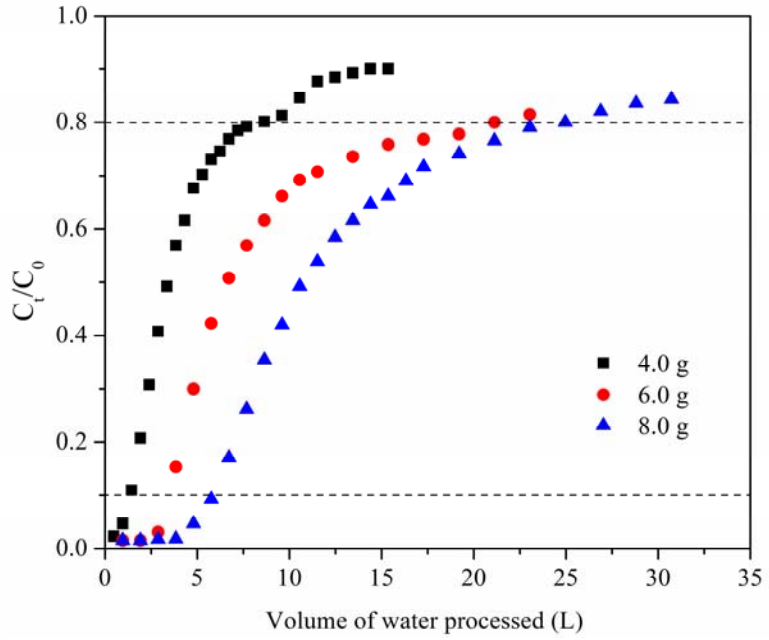

Fig. 1. Measured breakthrough curves showing fluoride adsorption on MgOP at different bed masses (4.0, 6.0 and 8.0 g). (Inlet fluoride concentration = 10 mg/L, volumetric flow rate = 16 mL/min, temperature = 30 °C).

Regression coefficients presented in Table 1 show that the Yan model described the breakthrough curves better than the Thomas model. Consequently, the plots of Yan model

predictions were closer to the experimental breakthrough curves than those of the Thomas model and better predicted critical operating parameters such as the breakthrough time, especially for low service time periods. This difference between the models' performance could be explained by the limitation of the Thomas model. In the experiments, the actual effluent concentration at $t = 0$ was not zero (contrary to the Thomas model estimate), and this inconsistency negatively affected the simulation of Thomas model, especially at low service time periods.

3.1.2 Volumetric flow rate

The effects on fluoride adsorption of various volumetric flow rates from 8 to 32 mL/min were conducted at a fixed inlet fluoride concentration of 10 mg/L and bed mass of 6.0 g. Increasing flow rate decreased the volume of effluent treated (Fig. 2). This is because the higher flow rate may have led to a lower residence time of the adsorbate in the column and consequently insufficient diffusion of the adsorbate into the pores of adsorbent. At the higher flow rates, the dynamic column capacity at the adsorbent exhaustion point was reduced as were the breakthrough time and exhaustion time. However, there was little change in the defluoridation capacity at the breakthrough time for flow rates from 8 to 16 mL/min.

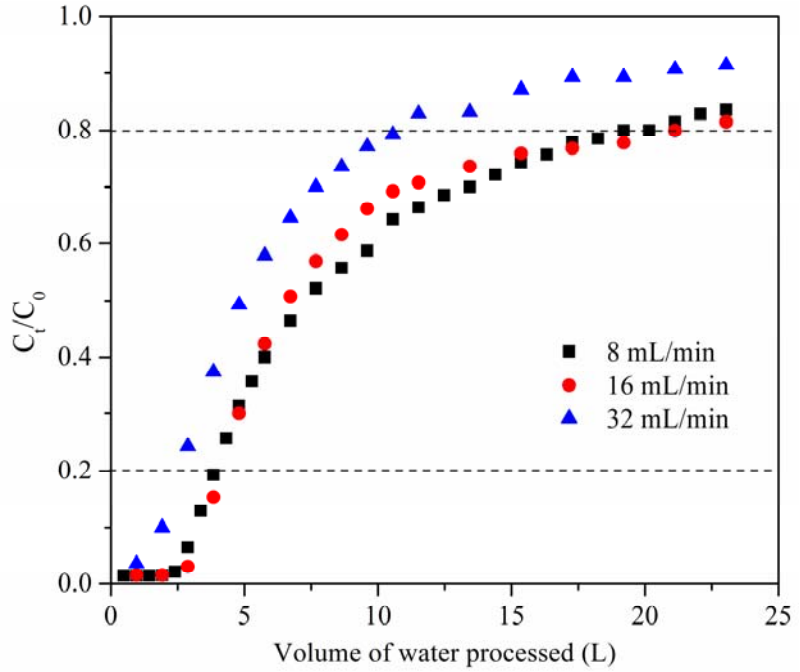

Fig. 2. Experimental breakthrough curves describing fluoride adsorption onto MgOP at different volumetric flow rates (8, 16 and 32 mL/min). (Inlet fluoride concentration = 10 mg/L, bed mass = 6.0 g, temperature = 30 °C).

Non-linear regression showed better agreement of the Yan model predictions with the fluoride removal data at various volumetric flow rates compared to the Thomas model (Table 1). The maximum adsorption capacity estimated by the Yan model (q_Y) and Thomas model (q_T) decreased at higher volumetric flow rate in accord with the experimental values (q_e). This phenomenon is likely due to insufficient time for diffusion and adsorption of fluoride onto the adsorbent at the higher flow rates.

3.1.3 Influent fluoride concentration

The effects of influent fluoride concentration on fluoride adsorption by MgOP were investigated. Breakthrough curves obtained at a bed mass of 6.0 g and flow rate of 16 mL/min are shown in Fig. 3. As the fluoride concentration increased from 5 to 20 mg/L, the breakthrough curves became progressively steeper, which indicated that the breakthrough

time and exhaustion time both decreased as the influent fluoride concentration increased. Similarly, the volume of water treated decreased from 5.8 to 0.9 L as the inlet fluoride concentration increased from 5 to 20 mg/L. The possible explanation for these results is that higher influent fluoride concentrations may have resulted in faster mass transfer of fluoride ions to MgOP because of the greater concentration gradient between the solution and MgOP surface, which provided a higher driving force for mass transfer. Consequently at the high influent fluoride concentrations, MgOP may have needed less time to become saturated, resulting in shorter breakthrough time and exhaustion time. However, there was little change in the defluoridation capacity of MgOP at the breakthrough point as the inlet fluoride concentration increased from 5 to 10 mg/L.

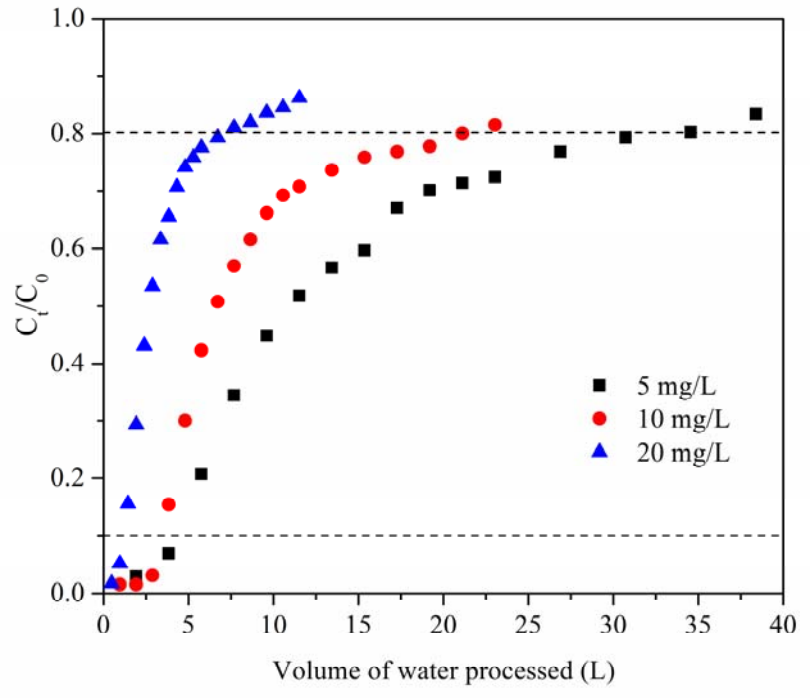

Fig. 3. Experimental breakthrough curves showing fluoride adsorption onto MgOP at different inlet fluoride concentrations (5, 10 and 20 mg/L). (Volumetric flow rate = 16 mL/min, bed mass = 6.0 g, temperature = 30 °C).

The maximum adsorption capacity estimated by the Yan model (q_Y) and Thomas model (q_T) indicated that the defluoridation capacity of MgOP reached a maximum when the influent fluoride concentration was maintained at 10 mg/L and the bed mass was fixed at 6.0 g.

3.1.4 Reaction temperature

The reaction temperature affects the volume of solution treated (or throughput volume) to a certain extent due to temperature-induced changes in the mass transfer of adsorbate. The breakthrough curves depicted in Fig. 4 show the effect of reaction temperature on fluoride adsorption at a bed mass of 6.0 g, volumetric flow velocity of 16 mL/min and influent fluoride concentration of 10 mg/L. The volume of water treated increased with increasing reaction temperatures from 20 to 40 °C. Moreover, the fluoride uptake at exhaustion time increased approximately 10% as the temperature increased from 20 to 40 °C.

Batch experiments in previous research (Kang et al., 2011) suggested that fluoride removal via MgOP is an endothermic chemisorption dominated reaction, an observation also made by other researchers (Asgari et al., 2012; Kameda et al., 2015; Wang et al., 2017). In agreement with theory, the results from the present study proved that the adsorption of fluoride on MgOP is indeed endothermic.

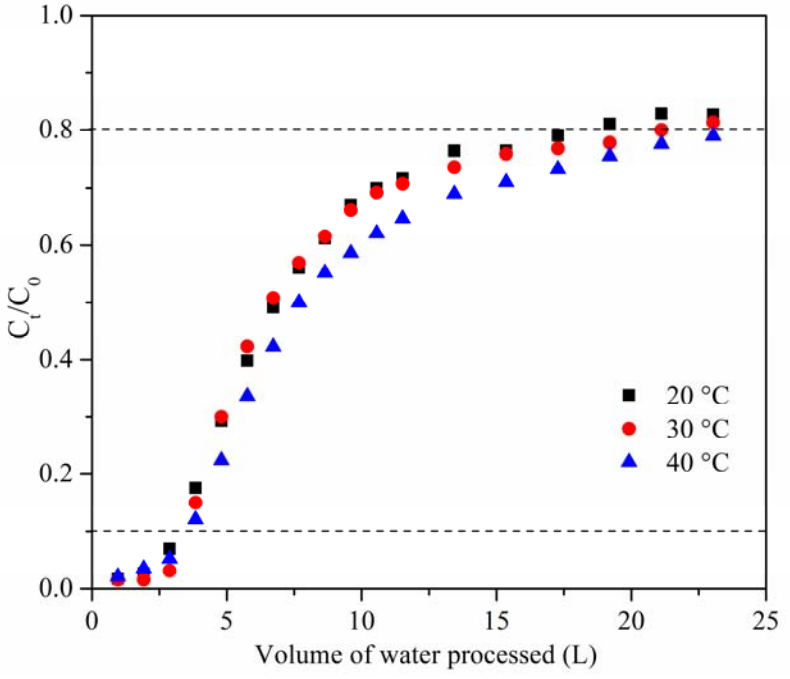

Fig. 4. Experimental breakthrough curves showing fluoride adsorption onto MgOP at different temperatures (20, 30 and 40 °C). (Inlet fluoride concentration = 10 mg/L, volumetric flow rate = 16 mL/min, bed mass = 6.0 g).

Data in Table 1 show that values for the kinetic rate constant in both the Yan model (k_Y)and Thomas model (k_T) decreased with increasing temperature. This trend reflected increases in the driving force of mass transfer with increasing temperature, a relationship corroborated by the increases in adsorption capacity at exhaustion point estimated by the Yan model (q_Y) and the Thomas model (q_T) with temperature, indicating a higher capacity for fluoride removal at higher temperature.

3.1.5 pH

Considering the alkalinity of MgOP, the pH of inlet fluoride solution is a factor strongly affecting the volume of fluoride solution that can be successfully treated. The breakthrough curves obtained from experiments at various influent pH values (4, 7, and 10) are presented in Fig. 5 for a fixed bed mass of 6.0 g, inlet flow rate of 16 mL/min and influent fluoride

concentration of 10 mg/L. In these experiments, the influent pH was adjusted by adding HCl and NaOH solutions. Fig. 5 shows that the volume of water treated was higher (4.2 L) at both low and high pH than at neutral pH (2.9 L). This result can be attributed to the change in the electrical charge of hydroxyl groups on the MgOP surface. The general principles of the surface chemistry of oxides in contact with an aqueous solution govern the behavior of amphoteric hydroxyl groups (Eqs. (7)–(9)):

$$-M-OH+H^{+}\rightarrow -M-OH_2^{+} \quad (7)$$

$$-M-OH_2^{+}+F^{-}\rightarrow -M-F+H_2O \quad (8)$$

$$-M-OH+F^{-}\rightarrow -M-F+OH^{-} \quad (9)$$

At low pH, fluoride ions are adsorbed mainly by the positively charged surface as indicated by Eqs. (7) and (8) (Loganathan et al., 2013; Singano et al., 1995). As the pH increases, fewer positively charged surfaces are acquired and fewer negatively charged fluoride ions are absorbed from the solution (Karthikeyan et al., 1997), resulting in decreasing adsorption capacity. At neutral pH, fluoride ions also can be adsorbed by ligand exchange even when the surface charge is neutral, as described by Eq. (9) (Choi and Chen, 1979). Thus, it is logical for adsorption capacity to decrease with increasing pH >7 due to the competition between fluoride and hydroxyl groups for the adsorption sites on the MgOP surface, as well as the greater number of hydroxyl groups in solution inhibiting ligand exchange (Eq. [9]). However, the opposite trend obtained from the experiments in this study indicated that the volume of treated fluoride solution increased from 2.9 L at pH 7 to 4.2 L at pH 10. Similarly, Singano et al. (1995) found that the optimized pH for the fluoride removal by MgO ranged from 10 to 11. This may be attributed to the surface chemistry of MgO such that a greater number of hydroxyl groups may increase the number of active adsorption sites on the MgOP surface at higher pH, thus improving fluoride adsorption. Furthermore, Vermilyea (1969) reported that the properties of MgO are similar to fine crystalline $Mg(OH)_2$

at higher pH. Because MgO is one of the raw material of the MgOP preparation and $Mg(OH)_2$ (with a finer crystalline matrix than MgO) could provide more surface area and/or active adsorption sites for fluoride adsorption, the fluoride adsorption could be enhanced with increasing pH. In contrast, batch experiments in previous research showed that the equilibrated defluoridation capacity of MgOP was negligibly affected when the pH ranged from 4 to 10 (Kang et al., 2011). Fluoride adsorption as a function of pH in the present study may be attributed to: a) a slower rate of MgOP dissolution at higher pH in the column, similar to observations in previous research (Pokrovsky and Schott, 2004), and b) shorter contact time of MgOP with fluoride ions in the dynamic experiment of the present study than in the batch study of previous research (Kang et al., 2011).

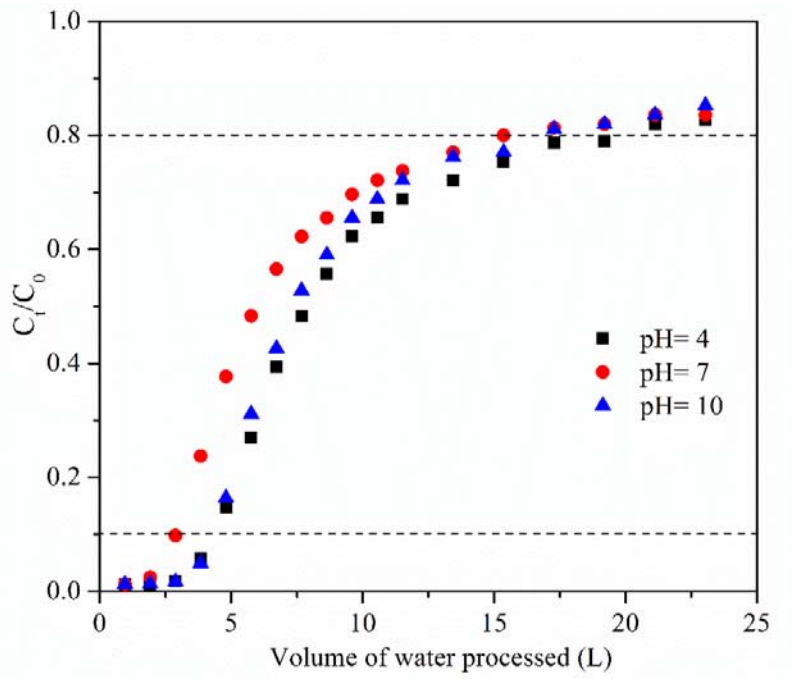

Fig. 5. Experimental breakthrough curves describing fluoride adsorption onto MgOP at different inlet pH values (4, 7 and 10). (Inlet fluoride concentration = 10 mg/L, volumetric flow rate = 16 mL/min, bed mass = 6.0 g, temperature = 30 °C).

411 Correlation coefficients presented in Table 1 show that the Yan model predicted fluoride
412 adsorption in the MgOP bed better than the Thomas model. Besides, the maximum adsorption
413 capacity estimated by the Yan model (q_Y) and Thomas model (q_T) was smallest at pH = 7,
414 reflecting the lower defluoridation capacity of MgOP at neutral pH.

415 **3.1.6 Coexisting anions**

416 The competitive effects of coexisting anions such as HCO_3^-, SO_4^{2-}, Cl^- and NO_3^- on the
417 fluoride adsorption in the MgOP bed also were investigated. The concentrations (0, 250 and
418 500 mg/L) of these coexisting anions were achieved by adding NaCl, Na_2SO_4, Na_2NO_3 and
419 $NaHCO_3$ solutions, respectively. Fluoride solution of fixed concentration (10 mg/L) was
420 passed through the individual columns containing 6.0 g of MgOP at a fixed volumetric flow
421 rate of 16 mL/min. Breakthrough curves for this experiment as shown in Fig. 6a and Fig. 6b
422 show that the volume of water processed that had an effluent fluoride concentration below the
423 permissible limit (1 mg/L) increased in the presence of Cl^- and SO_4^{2-} ions. This result may be
424 explained by the fact that the addition of Cl^- and SO_4^{2-} ions could accelerate dissolution of
425 the MgOP, thereby providing fresh sites for adsorption and thus improving fluoride removal.
426 However, increasing the concentrations of Cl^- and SO_4^{2-} ions from 250 to 500 mg/L
427 insignificantly affected the adsorption capacity of MgOP for fluoride ions, indicating that the
428 positive effects of such coexisting ions on fluoride adsorption may not be enhanced when the
429 concentrations of these coexisting anions exceed 250 mg/L.

430 The presence of NO_3^- showed minor influence on the breakthrough curves over the
431 concentration range of NO_3^- ions investigated (0–500 mg/L) (Fig. 6c). These results occurred
432 because NO_3^- ions as the low-affinity ligands are adsorbed through weaker bonds of outer-
433 sphere complexation and thus do not disturb the fluoride adsorption (Huang et al., 2011). The
434 batch experiment of fluoride adsorption on MgOP in previous research observed similar
435 results (Kang et al., 2011). However, when HCO_3^- ions were present at high concentrations,

436 the defluoridation capacity of MgOP at exhaustion point was reduced (Fig. 6d). Even though
437 the addition of HCO_3^- ions could cause a shift in pH to >8, and thus improve the fluoride
438 adsorption, these ions may also compete with fluoride ions for the active adsorption sites on
439 the MgOP surface. Many studies have also revealed the detrimental effects of HCO_3^- ions on
440 the fluoride adsorption, which may be attributed to the competition of fluoride and
441 bicarbonate ions for the active sorption sites, the pH change caused by the addition of
442 bicarbonate ions, or a combination of these effects (Maliyekkal et al., 2008; Xu et al., 2011;
443 Zhu et al., 2009). In the present study, the competitive effects may have had more influence
444 on fluoride adsorption in the column than the effects caused by the pH increase.
445
446
447

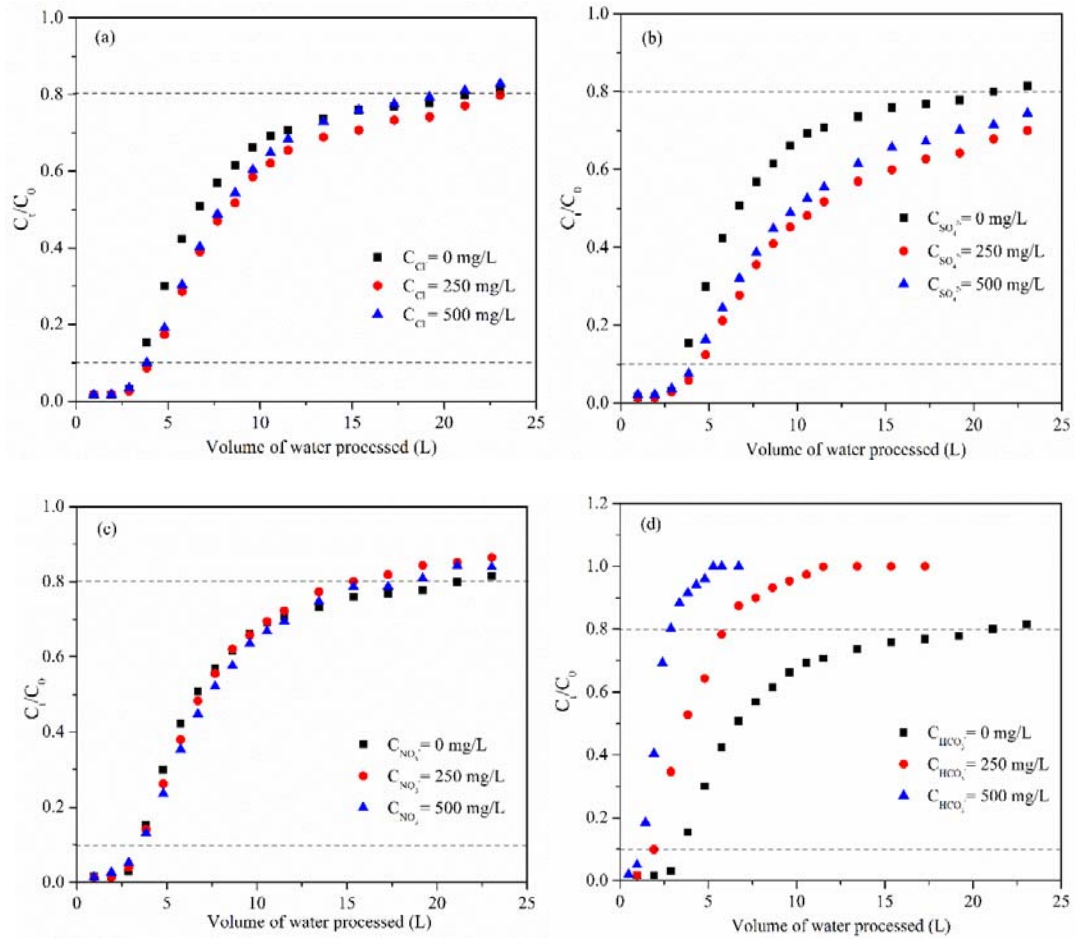

448 **Fig. 6.** Experimental reakthrough curves describing fluoride adsorption onto MgOP in the

449 presence of various concentrations (0, 250 and 500 mg/L) of different coexisting anions: (a)
450 Cl^- (b) SO_4^{2-} (c) NO_3^- (d) HCO_3^-. (Inlet fluoride concentration = 10 mg/L, volumetric flow
451 rate = 16 mL/min, bed mass = 6.0 g, temperature = 30 °C).
452
453 The regression coefficients (Table 1) for the Thomas model were lower than those of the
454 Yan model in the presence of all anions evaluated except for HCO_3^- ions. Because higher
455 values of maximum adsorption capacity estimated by the Thomas model (q_T) and the Yan
456 model (q_Y) showed better fluoride adsorption, it is obvious that the coexisting anions in
457 solution (especially the presence of SO_4^{2-}), led to increased defluoridation capacity of MgOP,
458 except for the adverse effects caused by the presence of HCO_3^-.

459 **3.2 Magnesium in treated water**

460 Magnesium is an essential element for human health, but the excessive intake of
461 magnesium can cause diseases called hypermagnesemia, such as gastrointestinal spasms,
462 myoparesis and asystole. The magnesium dissolution from MgOP was monitored in the
463 treated water by measuring the magnesium concentration in the effluent at a bed mass of 6.0
464 g, flow velocity of 16 mL/min and inlet fluoride concentration of 10 mg/L. The experiments
465 also were conducted at influent pH ranging from 4 to 10. Results showed that the
466 concentration of magnesium ions transferred to the solution remained in the range 1.0 to 2.0
467 mg/L. Since a magnesium concentration > 36 mg/L will lead to hypermagnesemia (Wyskida
468 et al., 2012), the adsorbent used in this study is considered to be safe for use in treating
469 drinking water when influent pH is in the range 4–10.

470 **3.3 Fluoride desorption and regeneration of MgOP**

471 Desorption and regeneration of MgOP increase the use efficiency and decrease
472 operational costs. Selection of a desorbing agent is very important and is determined by
473 MgOP structure and the mechanism of fluoride adsorption. The results of the desorption

474 experiments in this study showed that the desorption efficiency of fluoride-loaded MgOP was
475 very low (< 10%) using either HCl, NaCl, NaOH, Na_2CO_3, $C_6H_8O_7$, $Na_3C_6H_5O_7$ or deionized
476 water as the desorbing solvents, but such solvents had regeneration efficiency ~40% for the
477 fluoride-loaded MgOP. In a previous batch study, increasing the influent fluoride
478 concentrations from 10 to 30 mg/L resulted in an increased equlibrium defluoridation
479 capacity at a fixed MgOP concentration of 2.0 g/L (Kang et al., 2011). This observation
480 indicated that the fluoride adsorption on MgOP achieved at the initial fluoride concentration
481 of 10 mg/L in the present study may not have reached saturation and that active adsorption
482 sites were available to adsorb additional fluoride ions.
483 Thus, the regeneration experiment, in fact, was designed to utilize the unsaturated
484 MgOP for secondary fluoride removal. In this case, deionized water had no effect on the
485 regeneration of fluoride-loaded MgOP; rather, the regeneration efficacy (approximately 40%)
486 was due to the unused adsorption sites on the fluoride-loaded MgOP surface. Therefore, the
487 regeneration experiment conducted utilizing deionized water was considered as the "control"
488 experiment and served as the basis for comparing regeneration experiments using other
489 desorbing agents. The regeneration efficacies of HCl, NaCl, NaOH, Na_2CO_3, $C_6H_8O_7$,
490 $Na_3C_6H_5O_7$ solutions for fluoride-loaded MgOP should discount the regeneration efficacy
491 obtained utilizing deionized water. Thus, because these desorbing agents demonstrated
492 regeneration efficacies only slightly in excess of 40% (that of deionized water), it was
493 concluded that these products had low regeneration efficiency (< 1%) for the fluoride-loaded
494 MgOP.
495 In contrast, calcination regenerated fluoride-loaded MgOP to 97% of its original
496 capacity. This result occurred because the structure of fluoride-loaded MgOP was changed
497 while being heated at 500 °C. In this case, new MgO-based material was formed having fresh
498 sites for fluoride removal.

The SEM, XRD and FTIR of the virgin MgOP and fluoride−loaded MgOP before and after calcination were studied. SEM images of virgin MgOP and fluoride-loaded MgOP before calcination were similar; both images showed the flake-shaped morphology of the MgOP particles. The flake-like structure of MgOP created a high specific surface area and thus facilitated effective fluoride adsorption. However, the SEM image of the fluoride-loaded MgOP after calcination showed that the adsorbent surface was covered by numerous fine particles.

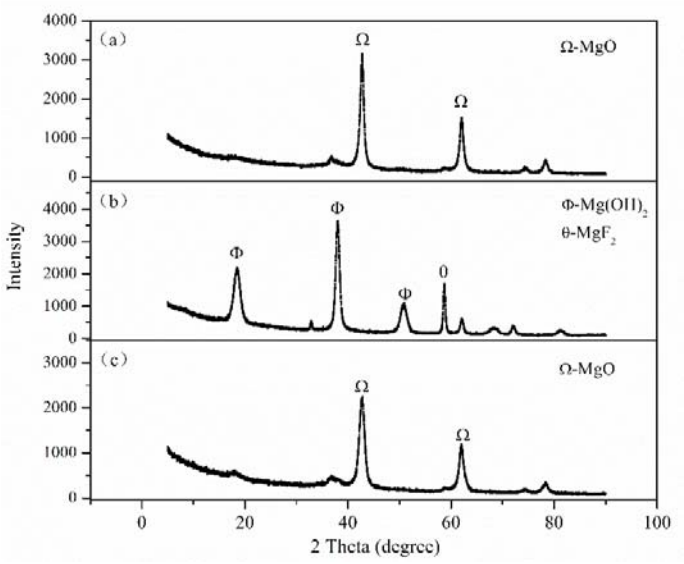

Fig. 7. X-ray diffraction patterns of (a) MgOP (b) fluoride-loaded MgOP before calcination (c) fluoride-loaded MgOP after calcination.

Powder XRD was used to determine the crystallinity and phase components of MgOP samples. The XRD pattern confirmed the presence of MgF_2 in fluoride-adsorbed MgOP (Fig. 7), which proved the successful adsorption of fluoride on MgOP. The XRD pattern of fluoride-loaded calcined MgOP heated at 500 °C presented similar peaks to those in the pattern of the material prior to calcination, but with less intensity as compared to the spectral peaks of virgin MgOP. The difference in intensity indicated that the content of MgO in the

517 fluoride-loaded MgOP after calcination was less than that in the original MgOP. Furthermore,
518 the formation of MgO in the fluoride-adsorbed MgOP may be attributed to the structural
519 destruction of fluoride-loaded MgOP. The possible pathway for the formation of MgO in the
520 fluoride-loaded MgOP after calcination is presented as the following sequence of reactions
521 (Souza et al., 2014).

522 $MgO + H_2O \rightarrow Mg(OH)_2$

523 $Mg(OH)_2 + F^- \rightarrow MgF_2 + OH^-$

524 $MgF_{2(s)} + H_2O \rightarrow MgF_2 \cdot H_2O_{\text{ (adsorbed)}}$

525 $MgF_2 \cdot H_2O_{\text{ (adsorbed)}} \rightarrow Mg(OH)F_{(s)} + HF_{(g)}$

526 $Mg(OH)F_{(s)} \rightarrow MgO_{(s)} + HF_{(g)}$

527

528 FTIR spectra (Fig. S1) were used to identify the presence of functional groups and types
529 of bonding. A peak appeared at 3427 cm^{-1}, which may be attributed to the stretching
530 vibration of hydroxyl groups from the water. However, the peak became stronger with an
531 increase of intensity in spectra, which may be attributed to the formation of the O–H···F
532 bond, and indicated the presence of hydrogen bonding. The spectra peaked at 1631 cm^{-1} due
533 to C=C bonding with the stretching vibration disturbed by the water molecules.

534 **4. Conclusions**

535 The fluoride adsorption on MgOP was investigated in a continuous fixed-bed column. A
536 dynamic study was used to provide theoretical and technical supports for the commercial
537 application of MgOP. The defluoridation capacity of MgOP increased in acid and alkaline
538 environments compared to the capacity at neutral pH. The HCO_3^- ions present in most natural
539 waters being treated may compete with fluoride ions for the adsorption sites and thus inhibit
540 the fluoride adsorption in a MgOP bed. Moreover, the Yan et al. (2001) model was better able
541 than the Thomas (1944) model to predict the adsorption behavior of fluoride ions in the

column. Magnesium concentrations in treated water were so low that MgOP can be deemed to be safe for drinking water treatment, thus increasing the technical feasibility of this technique. The regeneration of fluoride-loaded MgOP can be effectively achieved through calcination. In summary, the column study of fluoride adsorption on MgOP confirms that MgOP is an effective and safe adsorbent for defluoridation of drinking water at plant-scale.

Acknowledgements

This work was financially supported by the National Natural Science Foundation of China (51409108) and National Natural Science Foundation of China (21177045).

References

Abdolali, A., Ngo, H.H., Guo, W., Zhou, J.L., Zhang, J., Liang, S., Chang, S.W., Nguyen, D.D., Liu, Y., 2017. Application of a breakthrough biosorbent for removing heavy metalsfrom synthetic and real wastewaters in a lab-scale continuous fixed-bed column. Bioresour. Technol.

Asgari, G., Roshani, B., Ghanizadeh, G., 2012. The investigation of kinetic and isotherm of fluoride adsorption onto functionalize pumice stone. J. Hazard. Mater. 217, 123-132.

Chai, L., Wang, Y., Zhao, N., Yang, W., You, X., 2013. Sulfate-doped Fe_3O_4/Al_2O_3 nanoparticles as a novel adsorbent for fluoride removal from drinking water. Water Res. 47, 4040-4049.

Chakrabortty, S., Roy, M., Pal, P., 2013. Removal of fluoride from contaminated groundwater by cross flow nanofiltration: Transport modeling and economic evaluation. Desalination 313, 115-124.

Choi, W.-W., Chen, K.Y., 1979. The removal of fluoride from waters by adsorption. Journal American Water Works Association 71, 562-570.

García-Sánchez, J., Solache-Ríos, M., Martínez-Miranda, V., Enciso-Perez, R., Arteaga-Larios, N., Ojeda-Escamilla, M., Rodríguez-Torres, I., 2017. Experimental study of the adsorption of fluoride by modified magnetite using a continuous flow system and numerical simulation. Process Saf. Environ. Prot. 109, 130-139.

Huang, Y.-H., Shih, Y.-J., Chang, C.-C., 2011. Adsorption of fluoride by waste iron oxide: The effects of solution pH, major coexisting anions, and adsorbent calcination temperature. J. Hazard. Mater. 186, 1355-1359.

Jadhav, S.V., Bringas, E., Yadav, G.D., Rathod, V.K., Ortiz, I., Marathe, K.V., 2015. Arsenic and fluoride contaminated groundwaters: a review of current technologies for contaminants removal. J. Environ. Manage. 162, 306-325.

Kameda, T., Oba, J., Yoshioka, T., 2015. Kinetics and equilibrium studies on Mg-Al oxide for

576 removal of fluoride in aqueous solution and its use in recycling. J. Environ. Manage. 156, 252-
577 256.
578 Kameda, T., Oba, J., Yoshioka, T., 2017. Removal of boron and fluoride in wastewater using
579 Mg-Al layered double hydroxide and Mg-Al oxide. J. Environ. Manage. 188, 58-63.
580 Kang, J., Li, B., Song, J., Li, D., Yang, J., Zhan, W., Liu, D., 2011. Defluoridation of water
581 using calcined magnesia/pullulan composite. Chem. Eng. J. 166, 765-771.
582 Karthikeyan, G., Meenakshi, S., Apparel, B., 1997. Defluoridation properties of activated
583 alumina, 2nd International Workshop on Fluorosis Prevention and Defluoridation of Water,
584 Edited by. Eli Dahi & Joan Maj Nielsen, pp. 19-25.
585 Loganathan, P., Vigneswaran, S., Kandasamy, J., Naidu, R., 2013. Defluoridation of drinking
586 water using adsorption processes. J. Hazard. Mater. 248, 1-19.
587 Maliyekkal, S.M., Shukla, S., Philip, L., Nambi, I.M., 2008. Enhanced fluoride removal from
588 drinking water by magnesia-amended activated alumina granules. Chem. Eng. J. 140, 183-192.
589 Mohan, S., Singh, D.K., Kumar, V., Hasan, S.H., 2017. Effective removal of Fluoride ions by
590 rGO/ZrO 2 nanocomposite from aqueous solution: Fixed bed column adsorption modelling and
591 its adsorption mechanism. J. Fluorine Chem. 194, 40-50.
592 Oladoja, N., Chen, S., Drewes, J., Helmreich, B., 2015. Characterization of granular matrix
593 supported nano magnesium oxide as an adsorbent for defluoridation of groundwater. Chem.
594 Eng. J. 281, 632-643.
595 Pokrovsky, O.S., Schott, J., 2004. Experimental study of brucite dissolution and precipitation
596 in aqueous solutions: surface speciation and chemical affinity control. Geochim. Cosmochim.
597 Acta 68, 31-45.
598 Reynolds, T.D., 1977. Unit operations and processes in environmental engineering. Brooks.
599 Roy, S., Das, P., Sengupta, S., 2017. Treatability study using novel activated carbon prepared
600 from rice husk: Column study, optimization using response surface methodology and

601 mathematical modeling. Process Saf. Environ. Prot. 105, 184-193.
602 Shen, J., Schäfer, A., 2014. Removal of fluoride and uranium by nanofiltration and reverse
603 osmosis: a review. Chemosphere 117, 679-691.
604 Shrivastava, B.K., Vani, A., 2009. Comparative study of defluoridation technologies in India.
605 Asian J. Exp. Sci 23, 269-274.
606 Singano, J., Mashauri, D., Dahi, E., Mtalo, F., 1995. Effect of pH on Defluoridation of Water
607 by Magnesite. Ngurdoto, Tanzania October 18-21, 1995, 39.
608 Souza, T., Luz, A., Pandolfelli, V., 2014. Magnesium fluoride role on alumina–magnesia
609 cement-bonded castables. Ceram. Int. 40, 14947-14956.
610 Sundaram, C.S., Viswanathan, N., Meenakshi, S., 2009. Defluoridation of water using
611 magnesia/chitosan composite. J. Hazard. Mater. 163, 618-624.
612 Thergaonkar, V., Nawalakhe, W., 1971. Activated magnesia for fluoride removal. Ind. J.
613 Environ. Health 16, 241-243.
614 Thomas, H.C., 1944. Heterogeneous ion exchange in a flowing system. J. Am. Chem. Soc. 66,
615 1664-1666.
616 Vermilyea, D.A., 1969. The dissolution of MgO and Mg $(OH)_2$ in aqueous solutions. J.
617 Electrochem. Soc. 116, 1179-1183.
618 Wang, H., Feng, Q., Liu, K., Li, Z., Tang, X., Li, G., 2017. Highly efficient fluoride adsorption
619 from aqueous solution by nepheline prepared from kaolinite through alkali-hydrothermal
620 process. J. Environ. Manage. 196, 72-79.
621 WHO, 2011. Guidelines for drinking-water quality. Geneva: world health organization.
622 Wyskida, K., Witkowicz, J., Chudek, J., Więcek, A., 2012. Daily magnesium intake and
623 hypermagnesemia in hemodialysis patients with chronic kidney disease. J. Ren. Nutr. 22, 19-
624 26.
625 Xu, X., Li, Q., Cui, H., Pang, J., Sun, L., An, H., Zhai, J., 2011. Adsorption of fluoride from

626 aqueous solution on magnesia-loaded fly ash cenospheres. Desalination 272, 233-239.
627 Yan, G., Viraraghavan, T., Chen, M., 2001. A new model for heavy metal removal in a
628 biosorption column. Adsorpt. Sci. Technol. 19, 25-43.
629 Ye, Y., Hu, Y., Hussain, Z., Li, X., Li, D., Kang, J., 2016. Simultaneous adsorptive removal of
630 fluoride and phosphate by magnesia-pullulan composite from aqueous solution. RSC Adv. 6,
631 35966-35976.
632 Zhu, P., Wang, H., Sun, B., Deng, P., Hou, S., Yu, Y., 2009. Adsorption of fluoride from aqueous
633 solution by magnesia-amended silicon dioxide granules. J. Chem. Technol. Biotechnol. 84,
634 1449-1455.